

A Parallel Fully Coupled Implicit Domain Decomposition Method for Numerical Simulation of Microfluidic Mixing in 3D

Journal:	<i>International Journal of Computer Mathematics</i>
Manuscript ID:	GCOM-2011-0311-B
Manuscript Type:	Original Article
Date Submitted by the Author:	21-Apr-2011
Complete List of Authors:	Hwang, Feng-Nan; National Central University, Department of Mathematics Cai, X; University of Colorado at Boulder, Department of Computer Science Cheng, Yu-Lun; National Central University, Department of Mathematics Tsao, Chia-Wen; National Central University, Mechanical Engineering
Keywords:	Navier-Stokes equations, Microfluidics, Fully implicit methods, Domain decomposition, Parallel processing

SCHOLARONE™
Manuscripts

RESEARCH ARTICLE

A Parallel Fully Coupled Implicit Domain Decomposition Method for Numerical Simulation of Microfluidic Mixing in 3D

Feng-Nan Hwang^a, Xiao-Chuan Cai^b, Yu-Lun Cheng^a, Chia-Wen Tsao^{c*}

^aDepartment of Mathematics, National Central University, Jhongli, 32001 Taiwan;

^bDepartment of Computer Science, University of Colorado, Boulder, CO 80309, USA;

^cDepartment of Mechanical Engineering, National Central University, Jhongli 32001, Taiwan

(submitted to *IJCM*, April 2011)

A parallel fully coupled implicit fluid solver based on a Newton-Krylov-Schwarz algorithm is studied for the simulation of microfluidic described by the three-dimensional unsteady incompressible Navier-Stokes equations. The popularly used fractional step method, originally designed for high Reynolds number flows, requires some modification of the invicid-type pressure boundary condition in order to reduce the divergence error near the wall, on the other hand, the fully coupled approach works well without any special treatment of the boundary condition for low Reynolds number microchannel flows. A key component of the algorithm is an additive Schwarz preconditioner, which is used to accelerate the convergence of a linear Krylov-type solver for the saddle point-type Jacobian systems. As a test case, we carefully study a three-dimensional passive serpentine micromixer and report the parallel performance of the algorithm obtained on a parallel machine with more than one hundred processors.

Keywords: Navier-Stokes equations; microfluidics; fully implicit methods; domain decomposition; parallel processing

AMS Subject Classification: 65H10; 65N30; 65N55; 76D0

1. Introduction

Mixing enhancement is crucially important in many branches of emerging microfluidic technologies. Several different types of micromixers are available or proposed. Generally speaking, the micromixers can be classified into two major groups [16, 27]. One of them is the so-called active micromixer, in which mixing is achieved by some external perturbation applied, for example, through the pressure field [25], by magneto-hydrodynamics [4], or through acoustic disturbances [1, 41]. The other group consists of passive micromixers, where mixing relies solely on diffusion or chaotic advection without importing external energy. In comparison with the active type, the passive-type micromixers are more popular due to several advantages, including efficient mixing performance, simple fabrication, and high integration level with other lab-on-a-chip applications. To optimize the mixing performance, the main goal of the design of passive micromixers is to increase the contact surface between two fluids and to decrease the diffusion path between

*Corresponding author. Email: hwangf@math.ncu.edu.tw (F.-N. Hwang), cai@cs.colorado.edu (X.-C. Cai), 962201005@cc.ncu.edu.tw (Y.-L. Cheng), cwttsao@ncu.edu.tw (C.-W. Tsao)

them by changing the microchannel geometry. The mixing enhancement techniques include using a staggered herringbone microchannel to create three-dimensional twisting flows inside the microchannel [12, 17, 20, 35, 39], placing obstacles inside the microchannel to create chaotic mixing [30, 33] or changing velocity profiles with various microchannel cross-section geometries [37].

Most of the numerical simulations are carried out by using commercial software packages; e.g., ANSYS CFX [23], COMSOL [36], Fluent [8] or CFD-ACE [33, 39]. These packages are easy to use because of the friendly interface, but are usually not parallel, or restricted to very small number of processors, and therefore can not be used for high fidelity simulations, which require very fine meshes and large number of processors. Recently, Glatzel et al. [15] evaluated the performance of some available computational fluid dynamics software packages with emphasis on microfluidic applications and concluded that there is a real need for faster and more accurate algorithms and software for microfluidic simulations on large-scale parallel computers. Thus, the aim of this paper is to investigate a fully parallel approach for solving incompressible Navier-Stokes (NS) equations, which is used to simulate the mixing of fluids in microsystems. We hope the algorithms and software developed in this paper will provide engineers with a more efficient approach for the design of microfluidic devices, and a scalable tool for understanding the physics of fluids at nano or micro level. As a numerical example to demonstrate the applicability of our fluid solver to microfluidic systems and to evaluate the performance on a parallel machine, we focus on a three-dimensional serpentine microchannel, which is the passive micromixing model proposed by Liu et al. [24].

In this paper, we develop and study some fully implicit methods that have recently gained in popularity [3, 5, 6, 11, 26, 28, 40], because they allow much larger time-step size compared to fully explicit or linearly implicit methods and they are more scalable on large scale parallel computers. Additionally they are able to accurately capture the nonlinear coupling between components, conserve more physical quantities, such as mass, momentum, or energy for a longer period of simulation time. As pointed out by the authors of [21], the inviscid-type pressure boundary condition in the classical temporal fractional step method, which is originally designed for high Reynolds number flows, needs to be modified in order to reduce the divergence error near the boundaries (See Figure 16.2 on page 517 [21]). On the other hand, the fully coupled implicit approach considered in this paper works well for both high Reynolds number laminar flows and lower Reynolds number microflows without changing the boundary condition. The price to pay is that we have to solve a nonlinear system at every time step. The inexact Newton method is one of the popular approaches for solving such nonlinear system arising from time-dependent PDE problems because of its robustness and fast convergence. The kernel of the Newton type method is the linear Jacobian solver, which is the most expensive part of the algorithm and the design of an efficient preconditioner is crucial for the success of the algorithm.

Our parallel algorithm is based on a Newton-Krylov-Schwarz (NKS) algorithm [7], which consists of three key ingredients: an inexact Newton method with backtracking as the nonlinear solver, a Krylov subspace method [31] as the linear solver for the Jacobian systems together with a parallel overlapping Schwarz domain decomposition based preconditioner [34, 38] to accelerate the convergence of the linear solver. The major advantage of NKS is that it is fully parallel, since one does not need to split the velocity and pressure fields. Furthermore, NKS is extendable to simulate other more complex full microsystems involving coupled electrical, mechanical, thermal, and fluid components.

The rest of this paper is organized as follows. In the next section, we briefly

mention the microfluidic model based on incompressible NS equations, followed by a description of a Newton-Krylov nonlinear solver, a parallel Schwarz preconditioner for the saddle-point type Jacobian system, and an overview of parallel micro-flow simulator. In Section 4, numerical results for three microfluidic mixing problems are presented. Concluding remarks are given in Section 5.

2. A model for incompressible micro-flows and their mixing

To simulate the motion of fluids in a microchannel, we consider the three-dimensional unsteady incompressible NS equations defined on a bounded domain Ω with the boundary $\Gamma = \Gamma_D \cup \Gamma_N$ [21],

$$\left\{ \begin{array}{l} \rho \left(\frac{\partial \mathbf{u}}{\partial t} + \mathbf{u} \cdot \nabla \mathbf{u} \right) - \nabla \cdot \boldsymbol{\sigma} = 0 \quad \text{in } \Omega \times (0, T), \\ \nabla \cdot \mathbf{u} = 0 \quad \text{in } \Omega \times (0, T), \\ \mathbf{u} = \mathbf{g} \quad \text{on } \Gamma_D \times (0, T), \\ \nabla \cdot \boldsymbol{\sigma} = 0 \quad \text{on } \Gamma_N \times (0, T), \\ \mathbf{u} = \mathbf{u}_0 \quad \text{in } \Omega \text{ at } t = 0, \end{array} \right. \quad (1)$$

where $\mathbf{u} = (u_1, u_2, u_3)^T$ is the velocity, ρ is the fluid density, and $\boldsymbol{\sigma}$ is the Cauchy stress tensor defined as $\boldsymbol{\sigma} = -p\mathbf{I} + \mu[(\nabla \mathbf{u}) + (\nabla \mathbf{u})^T]$, where p is the pressure, \mathbf{I} is a second-order identity tensor, and μ is the dynamic viscosity. Here, we impose two types of boundary conditions: the Dirichlet boundary condition on Γ_D and the homogenous Neumann boundary condition on Γ_N and assume that the flow is stationary at the beginning of computation. The Reynolds number, Re , is defined as $\rho(Q/A)D_h/\mu$, where Q is the volumetric flow rate through the channel, A is the cross-sectional area, and $D_h = 4A/P$ (P is the wetting perimeter of the channel) is the hydraulic diameter of the channel. The Reynolds number is quite low in a microfluidic system, typically ranging from 0.01 to 100 [27]. However, due to the presence of some abrupt turns in the computational domain, e.g., a 3D micromixer, the effect of the convective acceleration term plays an important role during the numerical simulation, thus the diffusive term can not be neglected. To measure the degree of mixing of fluids, we solve a 3D convection-diffusion equation at certain time steps,

$$\mathbf{u} \cdot \nabla C - D \Delta C = 0, \quad (2)$$

where \mathbf{u} is the velocity field obtained from the solution of the NS equations, D is the diffusivity coefficient of the species, and C is the concentration of the species. The corresponding mixing efficiency at a cross-section of a channel is defined as

$$M = 1 - \sqrt{\frac{1}{n_c} \sum_{i=1}^{n_c} \left(\frac{C_i - \bar{C}}{\bar{C}} \right)^2}, \quad (3)$$

where n_c is the number of mesh points on the cross-section, C_i is the concentration at the mesh point and $\bar{C}(= 0.5)$ is the average number of concentration.

1 3. A parallel fully coupled and fully implicit fluid solver

2 Our parallel time-dependent 3D incompressible fluid solver is implemented on top
 3 of the Portable, Extensible Toolkit for Scientific Computation (PETSc) [2]. The
 4 solver has been validated and successfully applied to blood flows in the arteries [19].
 5 In addition, the parallel fluid solver has been integrated with other state-of-the-
 6 art pre-processing and post-processing software packages, including (1) Cubit [9]
 7 for 3D unstructured finite element mesh generation; (2) ParMETIS [22] for mesh
 8 partitioning for the purpose of parallel processing; (3) ParaView [29] for scientific
 9 visualization of numerical results and conducting data analysis. Below we give a de-
 10 scription of the discretization scheme and the parallel solution algorithm employed
 11 in the fluid solver.

12 To discretize the NS equations (1), we use an implicit backward Euler finite dif-
 13 ference method for the temporal variable and a stabilized $P_1 - P_1$ Galerkin/least-
 14 squares finite element method [13] in the spatial domain covered by a given tetra-
 15 hedral mesh. At each time step, it is necessary to solve a large, sparse, nonlinear
 16 algebraic system

21
$$F(x) = 0, \quad (4)$$

22 where the vector x corresponds to the nodal values of $\mathbf{u}_h = (u_h^1, u_h^2, u_h^3)$ and p_h at
 23 the time $t = (n + 1)\Delta t$. Here, only a uniform time step Δt is considered. To solve
 24 the nonlinear algebraic system a NKS algorithm is employed as follows. Let $x^{(0)}$
 25 be a given initial guess, which is taken from the velocity and pressure solutions at
 26 the previous time step and assume $x^{(k)}$ is the current approximation of the exact
 27 solution x^* . Then a new approximation $x^{(k+1)}$ can be computed via the following
 28 steps:

29 **Step 1:** Find a Newton direction $s^{(k)}$ by solving the following preconditioned
 30 Jacobian system approximately by a Krylov subspace method, such as the Gen-
 31 eralized minimal residual method (GMRES) [32],

32
$$J_k M_k^{-1} y = -F(x^{(k)}), \text{ with } s^{(k)} = M_k^{-1} y, \quad (5)$$

33 where J_k is the Jacobian of F evaluated at $x^{(k)}$ and the additive Schwarz pre-
 34 conditioner, M_k^{-1} , is defined in detail below.

35 **Step 2:** Obtain the new approximation $x^{(k+1)} = x^{(k)} + \lambda^{(k)} s^{(k)}$, where $\lambda^{(k)} \in$
 36 $(0, 1]$ is a damping parameter used to enhance the robustness of Newton type
 37 methods [10].

38 Here we define the additive Schwarz preconditioner. Let $\{\Omega_i^h, i = 1, \dots, N\}$ be a
 39 non-overlapping subdomain partition whose union covers the entire domain Ω and
 40 its mesh \mathcal{T}^h . To simplify the implementation, each subdomain problem is assigned
 41 to a single processor of the parallel computer. We denote by \mathcal{T}_i^h as the collection of
 42 mesh points in Ω_i^h . To obtain overlapping subdomains, we expand each subdomain
 43 Ω_i^h to a larger subdomain $\Omega_i^{h,\delta}$ with the boundary $\partial\Omega_i^{h,\delta}$. Here δ is an integer
 44 indicating the level of overlap. We assume that $\partial\Omega_i^{h,\delta}$ does not cut any elements
 45 of \mathcal{T}^h . Similarly, we denote by $\mathcal{T}_i^{h,\delta}$ as the collection of mesh points in $\Omega_i^{h,\delta}$. We
 46 define the additive Schwarz preconditioner for the Jacobian system, which is an
 47 extension of that for the saddle-point type Stokes equations as follows [18]. First

1 we introduce the subdomain velocity space
 2

$$3 \quad V_i^h = \{ \mathbf{v}^h \in V^h \cap (H^1(\Omega_i^{h,\delta}))^3 : \mathbf{v}^h = 0 \text{ on } \partial\Omega_i^{h,\delta} \}$$

4 and the subdomain pressure space
 5

$$6 \quad P_i^h = \{ p^h \in P^h \cap L^2(\Omega_i^{h,\delta}) : p^h = 0 \text{ on } \partial\Omega_i^{h,\delta} \setminus \Gamma_D \},$$

7 where V^h and P^h are the linear finite element spaces defined on the domain Ω
 8 for the velocity and the pressure, respectively. $L^2(\Omega)$, and $H^1(\Omega)$ are the standard
 9 notations with the usual meanings in the finite element literature [13, 14]. On the
 10 physical boundaries, we impose the Dirichlet condition according to the original
 11 equations (1). On the artificial boundaries, we assume both $\mathbf{u} = 0$ and $p = 0$.
 12 Similar boundary conditions were used in [18].

13 Let $R_i : V^h \times P^h \rightarrow V_i^h \times P_i^h$ be a global-to-local restriction operator, which
 14 returns all degrees of freedom (both velocity and pressure) associated with the
 15 subspace $V_i^h \times P_i^h$. R_i is an $4n_i \times 4n$ matrix with values of either 0 or 1, where
 16 n and n_i are the total number of mesh points in \mathcal{T}^h and $\mathcal{T}_i^{h,\delta}$, respectively, and
 17 $\sum_{i=1}^N 4n_i \geq 4n$. Note that for linear elements, we have four variables per mesh
 18 point, three for the velocity and one for the pressure. Then, the local-to-global
 19 interpolation operator R_i^T can be defined as the transpose of R_i . Using the restric-
 20 tion and interpolation operators, we write the additive Schwarz preconditioner in
 21 the matrix form as
 22

$$23 \quad M_k^{-1} = \sum_{i=1}^N R_i^T J_i^{-1} R_i,$$

24 where J_i^{-1} is subspace inverse of $J_i = R_i J R_i^T$. We remark that the multiplica-
 25 tion of R_i (and R_i^T) with a vector does not involve any arithmetic operation,
 26 but does involve communication in a distributed memory parallel implementation.
 27 The restriction operator R_i collects the data from neighboring subdomains, and
 28 the local-to-global prolongation operator R_i^T sends partial solution to neighboring
 29 subdomains. In practice, to save the computational cost and the memory use, the
 30 J_i^{-1} in M_k^{-1} are often replaced by an inexact solver, such as an incomplete LU
 31 decomposition (ILU) with some levels of fill-ins.

44. Numerical results and discussions

45 We report the simulation results for the three-dimensional serpentine microchannel
 46 flows together with a straight micorchannel and a square-wave microchannel for
 47 the purposes of comparison; see Fig. 1 for the geometrical configurations for these
 48 three test cases. Note that only one unit for each case is shown in the figure
 49 and the microchannel geometric models are constructed by connecting these units
 50 repeatedly. The number of units are selected so that the traveling paths for each
 51 case are roughly the same.

52 The simulations are performed using $np = 64$ starting from $t = 0$ and finishing at
 53 $t = 10$ with $\Delta t = 0.1$. Detailed information for the three test cases are summarized
 54 in Table 1. The mesh size for each case roughly equals to 0.1.

55 All numerical simulations are performed on the Vger PC cluster with a peak
 56 performance of 5184 Gflop/s at the National Central University in Taiwan. The
 57

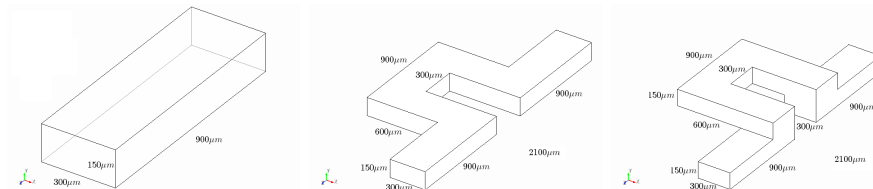


Figure 1. The dimensions of three microchannel models (only one unit is shown). From left to right: 1D straight, 2D square-wave, and 3D serpentine.

Table 1. Detailed information of three test cases.

system consists of 108 compute nodes, and each node has two Intel Xeon 3.0 GHz Dual-Core processor with 4 GB memory. The nodes are interconnected by a InfiniBand switch. All computations are done in double precision. The execution time is reported in seconds. The Jacobian matrices are constructed by a hybrid approach; i.e., all the linear terms and nonlinear terms associated with the Galerkin formulation are computed analytically, other stabilization terms are approximated by multicolored finite differences.

At each time step, we employ NKS to solve (4) with the previous time step solution as the initial guess. We claim the intermediate solution converges when the stopping condition for Newton

$$\|F(x^{(k)})\| \leq \max\{10^{-6}\|F(x^{(0)})\|, 10^{-10}\}$$

is satisfied. A cubic linesearch technique [10] is employed to determine the step length $\lambda^{(k)}$. Note that the previous time step solution is a good initial guess for most cases so that the line search procedure is seldom invoked. A right additive Schwarz preconditioned GMRES with a zero initial guess is employed to solve the Jacobian system. The accuracy of the solution to the Jacobian system is controlled by the stopping condition

$$\|F(x^{(k)}) + (J_k(x^{(k)})M_k^{-1})(M_k s^{(k)})\| \leq \max\{10^{-4}\|F(x^{(k)})\|, 10^{-10}\}.$$

Due to the nature of convection-dominated characteristic (typical Peclet number ranges from 10^2 to 10^5), the Galerkin/least squares finite element method is employed to discretize the equation (2), where the stabilization parameter employed is the one suggested by Franca et al. [14]. The corresponding linear system is solved by one-level additive Schwarz preconditioned GMRES, with the LU decomposition as the subdomain solver.

4.1 Simulation results

The fluids in the channel are assumed to be stationary at $t = 0$. At the beginning of the numerical simulation, two fluids with the same velocity are injected into a single microchannel and they merge at the vertical middle line at the inlet. The concentration of the left stream is set to be 0 (blue) and the right stream is set to be 1 (red) as the inlet boundary condition for the concentration in (2) and the homogenous Neumann boundary condition is imposed on the wall and at the

outlet. Such condition implies that there is no mixing taken place before entering the micromixer. Note that it is observed that the flow in the 3D serpentine channel reaches the quasi-steady state at around $t = 2$ for the case of $Re = 6$ and $t = 6$ for the case of $Re = 70$.

Fig. 2 displays the concentration distribution in each microchannel at $t = 2$ for the case of $Re = 6$. Due to the nature of laminar flows in the micro-scale channel, mixing relies mainly on diffusion. As shown on the top picture of Fig. 2, two fluid streams move forward smoothly along the 1D straight channel without any fluid perturbation involved and mixing occurs only along the interface of the two fluids near the middle of the channel. The situation is improved for the 2D square-wave micromixer (the middle picture of Fig. 2), the fluids skewing at the 90 degree turn result a larger contact surface area at the fluid interface. This induces a better mixing. This can be seen clearly from the left column of Fig. 3, which shows the concentration contours at different viewing windows. About 1/3 of the area of the cross-section is the complete mixing region (green area in the middle) near the outlet of the channel. Finally, both the bottom picture of Fig. 2 and the right column of Fig. 3 suggest that in the 3D serpentine micromixer, chaotic advection occurs, which greatly increases the contact surface area and shortens the mixing path between the two fluids, in other words, the mixing performance is significantly improved. Superior mixing performance is observed at the cross-section near the outlet of the 3D serpentine microchannel.

Figs. 4 and 5 show a comparison of the streamlines and the pressure distribution in the 1D straight, 2D square-wave and 3D serpentine microchannel at $t = 6$ for the case of $Re = 70$. It should be noted that the visualization of the streamlines is useful for studying the dead volume or eddies in the microchannel. And the pressure drop is of interests to the engineers, as it provides important information about the pump needed to drive the flow in the micro-device.

4.2 Impact of the viscosity

We next evaluate the mixing performance of the serpentine microchannel with respect to different values of Reynolds number, which is measured by the volumetric flow rate Q through the channel ranging from 0.1 mL/min to 1.2 mL/min. The mixing efficiency defined in (3) at a cross-section is used as the metric. Note that the total number of mesh points n_c on the cross-section is about 500. We show in Fig. 6 that the computed mixing efficiency at different viewing windows for four different values of the Reynolds number. It is clear that the mixing efficiency increases as the fluids flow toward the downstream direction and is at least 70% for all four cases when the fluids reach the 10th viewing window. As expected, the higher Reynolds number implies the better mixing efficiency. Similar observation obtained from experiments was also reported in [24].

4.3 Parallel performance of the algorithm

To achieve the optimal performance of the parallel fluid solver in terms of the computing time, several parameters need to be well tuned. Particularly, in this section, we study how the algorithmic parameters involved Krylov-Schwarz algorithms, as well as some physical parameters, effect the overall performance of the algorithm applied to the microchannel flows. These parameters include the number of levels of ILU fill-ins, the degree of overlap for the additive Schwarz preconditioner, the geometric configuration of the microchannel, and the Reynolds number. Such a study provides a guideline that helps the users to choose appropriate parameters

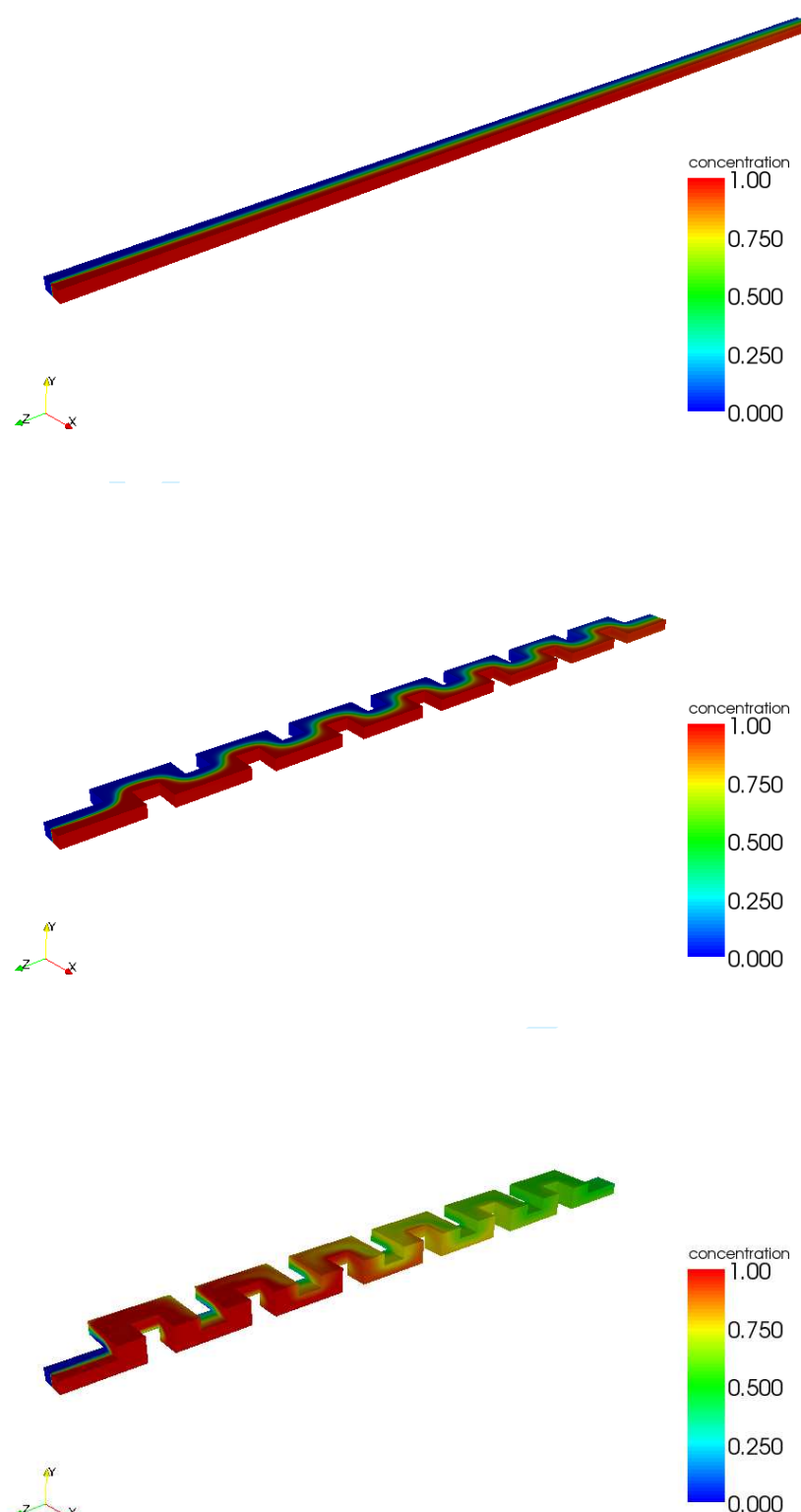


Figure 2. Concentration distribution in each microchannel for the case of $Re = 6$ at time $t = 2$. From top to bottom : 1D straight, 2D square-wave, and 3D serpentine.

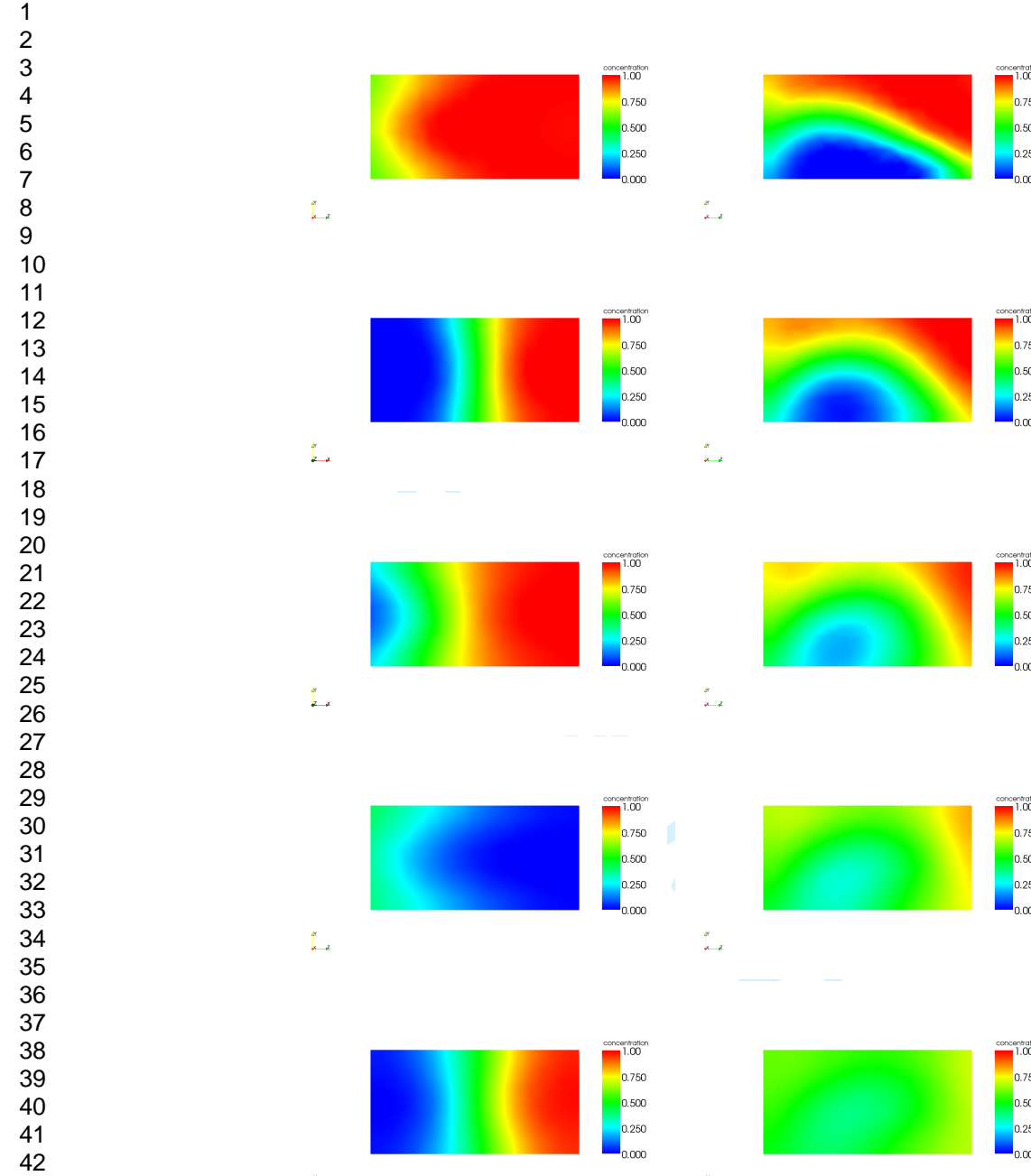


Figure 3. Concentration contours for 2D and 3D microchannels at the viewing windows 2, 4, 6, 8, and 10 at $t = 2$ from top to bottom. $Re = 6$ is considered. 2D (left) and 3D (right).

in their numerical simulations. Note that the number of levels of ILU fill-ins and the degree of overlap are related to the solution quality of the subdomain problem, which affects significantly the overall performance. Since solving the subdomain problem is the most time-consuming step in the algorithm, our goal is to reduce the effort on the subdomain solution as much as possible but not to degrade too much the convergence rate of the Krylov subspace method. Timing results reported in this section are obtained by running the simulation for 10 time steps. The total execution time, the average number of nonlinear iterations per time step (ANNI), the average number of linear iterations per Newton iteration (ANLI) are reported for the case of $Re = 6$ and $Re = 70$ in Table 2. As expected, the more ILU fill-ins

10

F.-N. Hwang, X.-C. Cai, Y.-L. Cheng, C.-W. Tsao

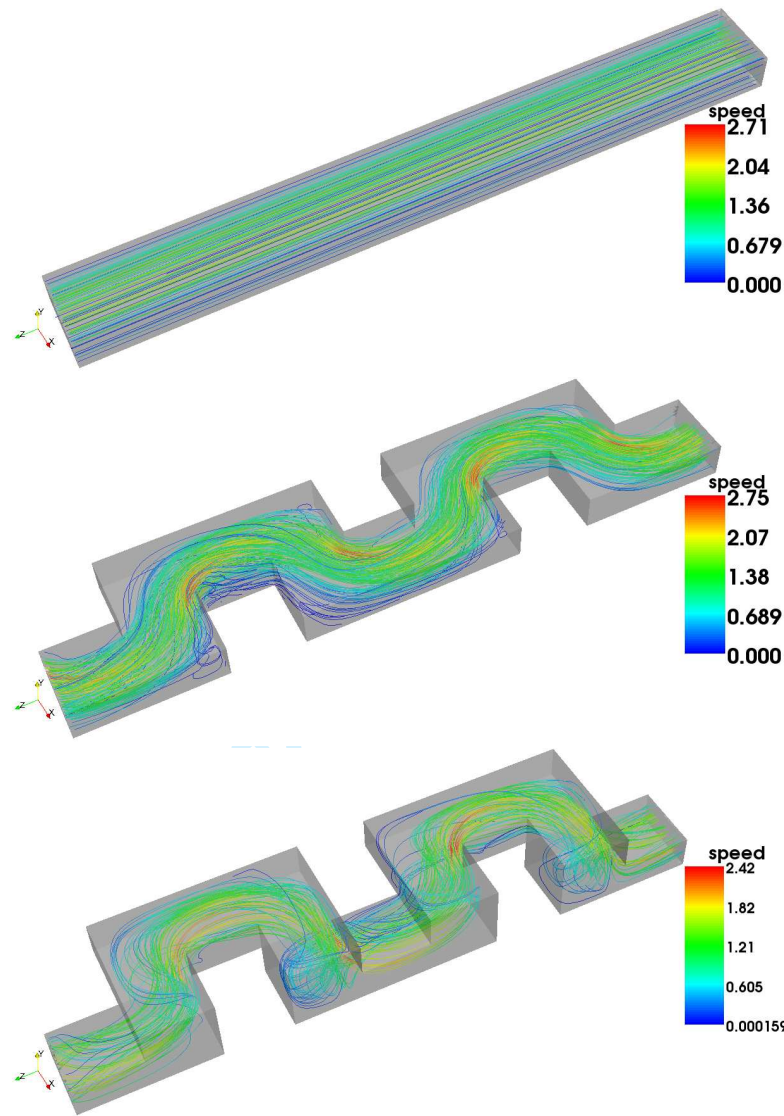


Figure 4. The streamlines for the 1D straight (top), the 2D square-wave (middle), and the 3D serpentine (bottom). Note that the last two units for all cases are shown in the figures.

and more overlap the fewer GMRES iterations are required to achieve the convergence. In these particular cases, ILU with a small number of fill-ins is too inexact to make the Schwarz preconditioner efficient. The same trends for both the 1D straight and 2D square-wave microchannels are also observed (not shown here). Furthermore, the communication cost is high, therefore we are not able to save any computing time by increasing the degree of overlap.

Next we summarize the timing results for three cases for $Re = 6$ and $Re = 70$ in Table 3. This table suggests that, generally speaking, the larger the Reynolds number is the more difficult it is for GMRES to converge. Without a coarse space, which may improve the communication between subdomains, the ANLI is usually high. Such a problem becomes more severe in the case of a long and thin computational domain like a microchannel even for a low Reynolds number flow with $Re = 70$. In many situations, Jacobian solves reach the maximum number of iterations, which is set to be 500. For the case of $Re = 6$, although the best choices for the level of ILU fill-ins and the degree of overlaps are slightly different, for example, $ovlp = 5$ and ILU(2) for 1D, $ovlp = 2$ and ILU(2) for 2D, and $ovlp = 1$ and ILU(3) for 3D, the number of GMRES iterations and the number of Newton iterations are quite

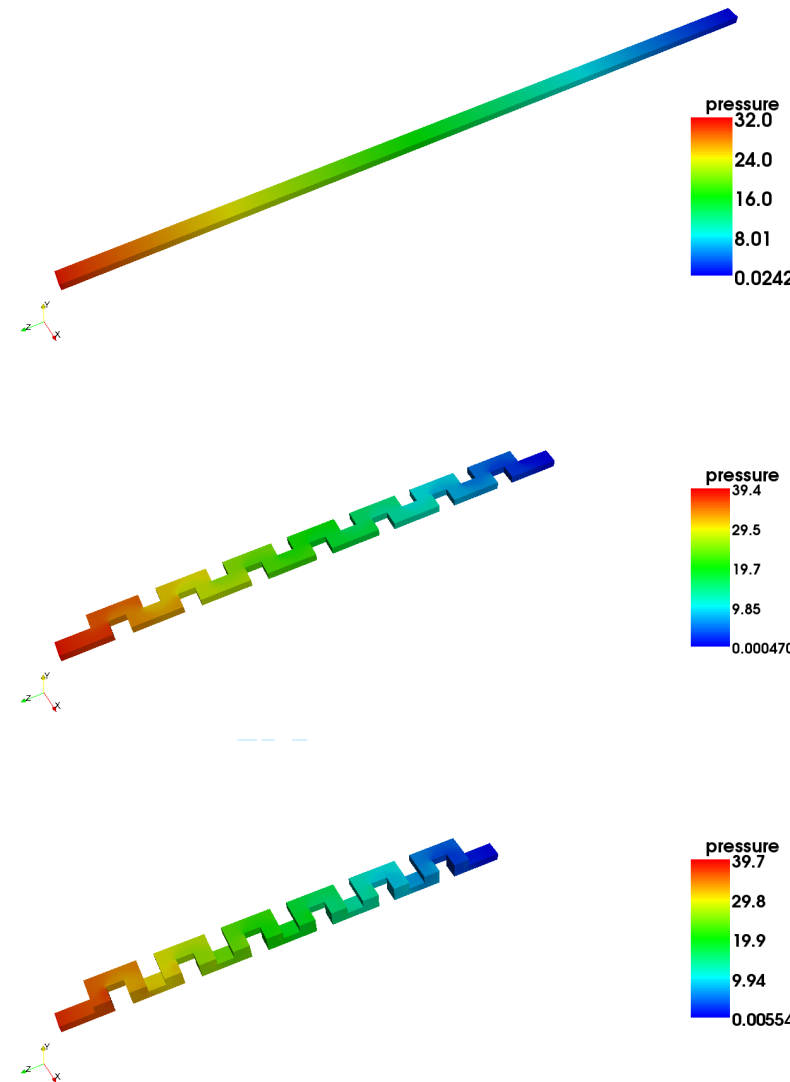


Figure 5. The pressure for the 1D straight (top), the 2D square-wave (middle), and the 3D serpentine (bottom).

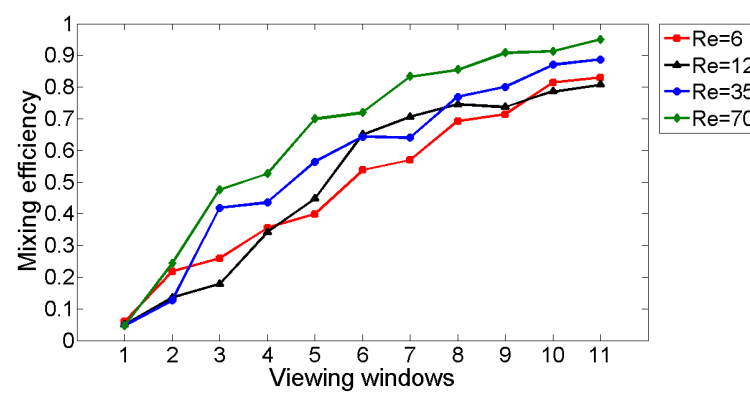


Figure 6. The mixing efficiency at different viewing windows for the cases with different values of the Reynolds number.

<i>Re</i> = 7		<i>ovlp</i> = 1	<i>ovlp</i> = 2	<i>ovlp</i> = 3	<i>ovlp</i> = 5
LU	ANNI (ANLI)	2.1 (131.3)	2.1 (122.0)	2.1 (119.6)	2.1 (107.0)
	Total time	875.4	1176.1	1447.8	2024.1
ILU(0)	ANNI (ANLI)	4.5 (495.4)	4.6 (495.7)	4.6 (496.0)	4.7 (496.1)
	Total time	931.4	991.3	1150.2	1256.6
ILU(1)	ANNI (ANLI)	2.8 (459.9)	2.8 (460.4)	2.8 (459.4)	2.3 (435.0)
	Total time	675.3	763.5	824.4	764.1
ILU(2)	ANNI (ANLI)	2.2 (359.5)	2.1 (320.2)	2.3 (232.1)	2.1 (186.1)
	Total time	574.1	581.4	553.6	510.7
ILU(3)	ANNI (ANLI)	2.1 (187.0)	2.1 (180.5)	2.1 (173.1)	2.1 (158.0)
	Total time	478.4	558.9	622.7	722.4
<i>Re</i> = 70		<i>ovlp</i> = 1	<i>ovlp</i> = 2	<i>ovlp</i> = 3	<i>ovlp</i> = 5
LU	ANNI (ANLI)	3.1 (382.6)	3.1 (176.4)	3.1 (163.7)	3.1 (136.6)
	Total time	2169.6	1981.0	2377.2	3200.9
ILU(0)	ANNI (ANLI)	7.1 (475.3)	7.2 (475.7)	7.2 (475.8)	6.9 (474.8)
	Total time	1266.6	1413.6	1506.5	1635.2
ILU(1)	ANNI (ANLI)	5.1 (461.2)	4.9 (461.4)	5.1 (460.2)	4.5 (454.3)
	Total time	1332.4	1501.7	1540.9	1688.6
ILU(2)	ANNI (ANLI)	4.0 (447.3)	4.0 (440.4)	3.9 (431.8)	3.5 (428.9)
	Total time	1229.6	1419.0	1521.5	1638.5
ILU(3)	ANNI (ANLI)	3.4 (434.5)	3.4 (424.5)	3.2 (404.1)	3.1 (389.7)
	Total time	1405.0	1672.2	1739.5	2040.8

Table 2. **3D serpentine micromixing.** Different subdomain solves: LU and ILU(k), $k = 0, 1, 2, 3$ for varied sizes of overlapping for $Re = 6$ and $Re = 70$. $\Delta t = 0.1$, 10 time steps are performed. $np = 64$.

independent of the geometric configurations of microchannels.

		1D	2D	3D
<i>Re</i> = 6	ANNI (ANLI)	2.1 (188.5)	2.1 (195.0)	2.1 (187.0)
	Total time	439.6	372.0	478.4
<i>Re</i> = 70	ANNI (ANLI)	5.5 (500)	3.3 (424.5)	3.4 (496.0)
	Total time	1361.6	1053.3	1405.0

Table 3. Timing results for three microchannel cases for $Re = 6$ and 70. $\Delta t = 0.1$, 10 time steps are performed

Finally, to evaluate the parallel performance of our fluid solver, we consider the parallel efficiency defined as

$$E_f = \left(\frac{16}{np} \right) \frac{T_{16}}{T_{np}},$$

where T_{16} and T_{np} are the computing time obtained with 16 and np processors.

From Tables 4 and 5, we observe that the parallel efficiency reaches at least 50% with up to 128 processors but degrades slightly when 256 processors are used.

5. Conclusions

In this work, we introduced a parallel algorithm for the 3D microfluidic simulation and the corresponding software was developed on top of PETSc and several state-of-the-art open source packages. The core of the approach is based on a fully coupled and fully implicit scalable Newton-Krylov-Schwarz method. Our studies showed

1	np	ANNI	ANLI	Time (secs)	Efficiency (%)
2	16	2.1	158.6	1587.3	100
3	32	2.1	163.5	877.3	90
4	64	2.1	187.0	478.4	83
5	128	2.2	264.2	370.0	54
6	256	2.4	394.2	317.5	31

Table 4. Parallel efficiency for the 3D serpentine micromixing case with $Re = 26$. The additive Schwarz preconditioner uses $ovlp = 1$ and ILU(3) as the subdomain solver.

10	np	ANNI	ANLI	Time (secs)	Efficiency (%)
11	16	4.7	456.8	3888.3	100
12	32	4.4	455.7	1989.9	98
13	64	5.1	461.2	1224.3	79
14	128	5.0	460.6	734.2	66
15	256	5.0	464.8	505.8	48

Table 5. Parallel efficiency for the 3D serpentine micromixing case with $Re = 70$. The additive Schwarz preconditioner uses $ovlp = 1$ and ILU(1) as the subdomain solver.

good qualitative agreements between numerical solutions and experimental data. Moreover, we used the three-dimensional serpentine microchannel as an numerical example to demonstrate the applicability of our software to the simulation of microfluidic mixing. Our solver achieved above 54% of parallel efficiency with up to 128 processors on a cluster of PCs.

References

- [1] D. Ahmed, X. Mao, J. Shi, B. Juluri, and T. Huang. A millisecond micromixer via single-bubble-based acoustic streaming. *Lab Chip*, 9:2738–2741, 2009. ISSN 1473-0197.
- [2] S. Balay, K. Buschelman, W. Gropp, D. Kaushik, M. Knepley, L. C. McInnes, B. Smith, and H. Zhang. PETSc Webpage, 2011. <http://www.mcs.anl.gov/petsc>.
- [3] A. Barker and X.-C. Cai. Scalable parallel methods for monolithic coupling in fluid-structure interaction with application to blood flow modeling. *J. Comput. Phys.*, 229:642–659, 2010.
- [4] H. Bau, J. Zhong, and M. Yi. A minute magneto hydrodynamic (MHD) mixer. *Sensor Actuator B Chem.*, 79:207–215, 2001. ISSN 0925-4005.
- [5] S. Behara and S. Mittal. Parallel finite element computation of incompressible flows. *Parallel Comput.*, 35:195–212, 2009.
- [6] P. Brown, D. Shumaker, and C. Woodward. Fully implicit solution of large-scale non-equilibrium radiation diffusion with high order time integration. *J. Comput. Phys.*, 204:760–783, 2005.
- [7] X.-C. Cai, W. Gropp, D. Keyes, R. Melvin, and D. Young. Parallel Newton-Krylov-Schwarz algorithms for the transonic full potential equation. *SIAM J. Sci. Comput.*, 19, 1998.
- [8] R. Choudhary, T. Bhakat, R. Singh, A. Ghubade, S. Mandal, A. Ghosh, A. Rammohan, A. Sharma, and S. Bhattacharya. Bilayer staggered herringbone micro-mixers with symmetric and asymmetric geometries. *Microfluid. Nanofluid.*, in press, 2011. ISSN 1613-4982.
- [9] Cubit. Online CUBIT user's manual, 2011. <http://cubit.sandia.gov/documentation.html>.
- [10] J. Dennis and R. Schnabel. *Numerical methods for unconstrained optimization and nonlinear equations*. SIAM, 1996.
- [11] W. Dettmer and D. Perić. An analysis of the time integration algorithms for the finite element solutions of incompressible Navier-Stokes equations based on a stabilised formulation. *Comput. Methods Appl. Mech. Engrg.*, 192:1177–1226, 2003.
- [12] Y. Du, Z. Zhang, C. Yim, M. Lin, and X. Cao. A simplified design of the staggered herringbone micromixer for practical applications. *Biomicrofluidics*, 4:024105, 2010.
- [13] L. Franca and S. Frey. Stabilized finite element methods. II: The incompressible Navier-Stokes equations. *Comput. Methods Appl. Mech. Engrg.*, 99:209–233, 1992.
- [14] L. Franca, T. Hughes, and S. Frey. Stabilized finite element methods: I. Application to the advective-diffusive model. *Comput. Methods Appl. Mech. Engrg.*, 95:253–276, 1992.
- [15] T. Glatzel, C. Litterst, C. Cupelli, T. Lindemann, C. Moosmann, R. Niekrawietz, W. Streule, R. Zengerle, and P. Koltay. Computational fluid dynamics (CFD) software tools for microfluidic applications-A case study. *Comput. Fluid.*, 37:218–235, 2008. ISSN 0045-7930.
- [16] V. Hessel, H. Löwe, and F. Schönfeld. Micromixers—a review on passive and active mixing principles. *Chem. Eng. Sci.*, 60:2479–2501, 2005.
- [17] S. Hossain, A. Husain, and K. Kim. Shape optimization of a micromixer with staggered-herringbone grooves patterned on opposite walls. *Chem. Eng. J.*, 162:730–737, 2010. ISSN 1385-8947.

1 [18] F.-N. Hwang and X.-C. Cai. Parallel fully coupled Schwarz preconditioners for saddle point problems. *Electron. Trans. Numer. Anal.*, 22:146–162, 2006.

2 [19] F.-N. Hwang, C.-Y. Wu, and X.-C. Cai. Numerical simulation of three-dimensional blood flows using 3 domain decomposition method on parallel computer. *J. Chin. Soc. Mech. Eng.*, 31:199–208, 2010.

4 [20] T. Kang, M. Singh, T. Kwon, and P. Anderson. Chaotic mixing using periodic and aperiodic sequences 5 of mixing protocols in a micromixer. *Microfluid. Nanofluid.*, 4:589–599, 2008.

6 [21] G. Karniadakis, A. Beşkök, and N. Aluru. *Microflows and Nanoflows: Fundamentals and Simulation*. 7 Springer Verlag, 2005.

8 [22] G. Karypis. METIS homepage, 2011. <http://cubit.sandia.gov/documentation.html>.

9 [23] L. Li, L. Lee, J. Castro, and A. Yi. Improving mixing efficiency of a polymer micromixer by use of a 10 plastic shim divider. *J. Micromech. Microeng.*, 20:035012, 2010.

11 [24] R. Liu, M. Stremler, K. Sharp, M. Olsen, J. Santiago, R. Adrian, H. Aref, and D. Beebe. Passive 12 mixing in a three-dimensional serpentine microchannel. *IEEE ASME J. Microelectromech. Syst.*, 9: 13 190–197, 2002.

14 [25] S. Müller, I. Mezi, J. Walther, and P. Koumoutsakos. Transverse momentum micromixer optimization 15 with evolution strategies. *Comput. Fluid.*, 33:521–531, 2004.

16 [26] M. Murillo and X.-C. Cai. A fully implicit parallel algorithm for simulating the non-linear electrical 17 activity of the heart. *Numer. Linear Algebra Appl.*, 11:261–277, 2004. ISSN 1099-1506.

18 [27] N.-T. Nguyen and Z. Wu. Micromixers—a review. *J. Micromech. Microeng.*, 15:R1–R16, 2005.

19 [28] S. Ovtchinnikov, F. Dobrian, X.-C. Cai, and D. Keyes. Additive Schwarz-based fully coupled implicit 20 methods for resistive Hall magnetohydrodynamic problems. *J. Comput. Phys.*, 225:1919–1936, 2007. 21 ISSN 0021-9991.

22 [29] ParaView. ParaView homepage, 2011. <http://www.paraview.org>.

23 [30] J. Park, K. Seo, and T. Kwon. A chaotic micromixer using obstruction-pairs. *J. Micromech. Microeng.*, 20:015023, 2010.

24 [31] Y. Saad. *Iterative methods for sparse linear systems*. SIAM, 2003. ISBN 0898715342.

25 [32] Y. Saad and M. Schultz. GMRES: A generalized minimal residual algorithm for solving nonsymmetric 26 linear systems. *SIAM J. Sci. Stat. Comput.*, 7:856–869, 1986.

27 [33] T.-R. Shih and C.-K. Chung. A high-efficiency planar micromixer with convection and diffusion 28 mixing over a wide Reynolds number range. *Microfluid. Nanofluid.*, 5:175–183, 2008.

29 [34] B. Smith, P. Bjørstad, and W. Gropp. *Domain Decomposition: Parallel Multilevel Methods for Elliptic 30 Partial Differential Equations*. Cambridge University Press, 1996.

31 [35] A. Stroock, S. Dertinger, A. Ajdari, I. Mezic, H. Stone, and G. Whitesides. Chaotic mixer for 32 microchannels. *Science*, 295:647–651, 2002.

33 [36] A. Tabak and S. Yesilyurt. Simulation-based analysis of flow due to traveling-plane-wave deformations 34 on elastic thin-film actuators in micropumps. *Microfluid. Nanofluid.*, 4:489–500, 2008. ISSN 1613- 35 4982.

36 [37] E. Tafti, R. Kumar, and H. Cho. Effect of laminar velocity profile variation on mixing in microfluidic 37 devices: The sigma micromixer. *Appl. Phys. Lett.*, 93:143504, 2008.

38 [38] A. Toselli and O. Widlund. *Domain Decomposition Methods-Algorithms and Theory*. Springer, 2005.

39 [39] K.-Y. Tung and J.-T. Yang. Analysis of a chaotic micromixer by novel methods of particle tracking 40 and FRET. *Microfluid. Nanofluid.*, 5:749–759, 2008.

41 [40] C. Yang, J. Cao, and X.-C. Cai. A fully implicit domain decomposition algorithm for shallow water 42 equations on the cubed-sphere. *SIAM J. Sci. Comput.*, 32:418–438, 2010.

43 [41] Z. Yang, S. Matsumoto, H. Goto, M. Matsumoto, and R. Maeda. Ultrasonic micromixer for microfluidic 44 systems. *Sensor Actuator Phys.*, 93:266–272, 2001. ISSN 0924-4247.

45

46

47

48

49

50

51

52

53

54

55

56

57

58

59

60